Journal of Engg. Research **Vol. 5 No. (2) June 2017 pp.** *129-140*

بحث تأثير السرعة على دقة الفحص لحساس الحث الكهربائي

وو يو، تشانغ هونغ بنغ، سون يو تشينغ و تشن هاي تشيوان

كلية هندسة الميكانيكيا البحرية، جامعة الملاحة البحرية بداليان، داليان، 116026، الصين

الخـــلاصـــة

بالنسبة إلى حساس الحث الكهربائي، تحدث الحركة النسبية بين ملف ثابت وهدف الفحص المعدني أو الملف الآخر، كما أن حساس الحث الكهربائي عادة يستعمل في قياسة الهدف المعدني بالتحرك والدوران والحركة المتكررة. لكن لم يبحث تأثير سرعة الحركة النسبية على دقة فحص حساس الحث الكهربائي. لذلك يبحث تأثير سرعة الحركة للحبيبات المعدنية على دقة فحص حساس الحث الكهربائي لتحسين أداء حساس الحث الكهربائي ورفع حساسية الفحص للحبيبات المعدنية وتطبيق حساس الحث الكهربائي في المجالات الأخرى. تبحث هذه الرسالة العلاقات بين سرعة حركة الحبيبات المعدنية ودقة فحص حساس الحث الكهربائي عبر التحليل النظري والتدقيق التجربي. تتمثل نتيجة التحليل في أنه يمكن رفع دقة الفحص للحساس عبر تخفيض سرعة الحبيبات المعدنية. عندما تنخفض سرعة الحبيبات المعدنية من $2.9\,m/s \times 10^{-2}$ إلى $5.8\,m/s \times 10^{-3}$، ترفع قيمة الحساس للملف من 0.43 nH إلى 0.81 nH وذلك يعني أن دقة الفحص ترفع بـ 87.5 %.

Research on the Influence of Velocity on the Sensitivity of Inductive Sensor

Yu Wu, Hongpeng Zhang*, Yuqing Sun and Haiquan Chen
Marine Engineering College, Dalian Maritime University, Dalian, 116026, China
**Corresponding Author: zhppeter@163.com*

ABSTRACT

In an inductive sensor, relative movement occurs between a fixed coil and a metal target or another coil, and inductive sensors are often used to measure moving, rotating and reciprocating targets. However, the effect of this relative movement on the detection capabilities of inductive sensors has not previously been investigated. Therefore, the influence of velocity on the sensitivity of inductive sensors for metal particle detection should be addressed to improve the performance of inductive sensors in terms of their sensitivity for metal particle detection and in other aspects of their operation. This paper presents a theoretical analysis and experimental validation of the dependence of the sensitivity of an inductive sensor on the velocity of the particles it is measuring. The results indicate that the sensitivity to particles can be significantly improved by decreasing their velocity. When the velocity of the particles is decreased from 2.9×10^{-2} m/s to 5.8×10^{-3} m/s, the inductance variation of the coil increases from 0.43 nH to 0.81 nH, corresponding to a sensitivity enhancement of 87.5%.

Keywords: Detection sensitivity; inductive sensor; measurement; particle detection; velocity.

INTRODUCTION

Inductive sensors have achieved considerable success because of their low manufacturing cost, high reliability, robustness, resistance to fouling and contact-free operation (Kim 2013; Kejik et al. 2004). The operating conditions of inductive sensors are less strongly affected compared to other types of sensors by environmental factors including humidity, temperature, dust, contamination and mechanical offsets (Bartsch et al. 2012; Rahal et al. 2009; Danisi et al. 2013; Wei et al. 2012). Therefore, they can be applied in certain harsh working environments. Inductive sensors are commonly used in industrial applications, such as in the detection of defects (Cha et al. 2010) or metal wear particles in lubrication oil (Du et al. 2010) or for measurements of temperature (Kim et al. 2000), pressure (Bakhoum et al. 2011; Bera et al. 2011), tip clearances (Du et al. 2014), forces (Du et al. 2015), metallic profiles (Passeraub et al. 1998), positions (Zhang et al. 2013; Aschenbrenner et al. 2015) and displacements (Tang et al. 2015; Coskun et al. 2013)

Relative movement typically occurs in an inductive sensor between a fixed coil and a metal target or another coil, and inductive sensors are often used to measure moving, rotating and reciprocating targets. However, the effect of this relative movement (or velocity) on the detection capabilities of inductive sensors has not previously been investigated. Therefore, the influence of velocity on the sensitivity of inductive sensors for metal particle detection should be addressed to improve the performance of inductive sensors in terms of their sensitivity for metal particle detection and in other areas of application.

In previous work, it has been found that identical particles traveling at different velocities induce different signals in inductive sensors. In other words, the particle velocity can be adjusted to enhance the sensitivity of an inductive sensor. This paper presents a theoretical analysis and experimental validation of the effect of particle velocity on the sensitivity of inductive sensors.

THE PRINCIPLE OF PARTICLE DETECTION

In the scenario illustrated in Figure 1(a), when an alternating current (AC) voltage is applied across the planar coil, a magnetic field is induced around the coil, and an induced electromotive force ε is generated in accordance with the Faraday's law of electromagnetic induction. Because the metal conductor forms a closed loop, eddy currents are generated. According to Lenz's law, the direction of the eddy current will oppose the change that produced it, and the electromotive force ε induced in the metal conductor can be expressed as

$$\varepsilon = -\frac{d\Phi}{dt} \tag{1}$$

A diagram of a microfluidic chip based on an inductive sensor is presented in Figure 1(b). When a high-frequency AC voltage is applied across the coil, eddy currents are generated in a metallic particle as it passes through the channel, and the magnetic field of these eddy currents, which opposes the magnetic field of the coil, is detected by the coil, causing a change in the inductance.

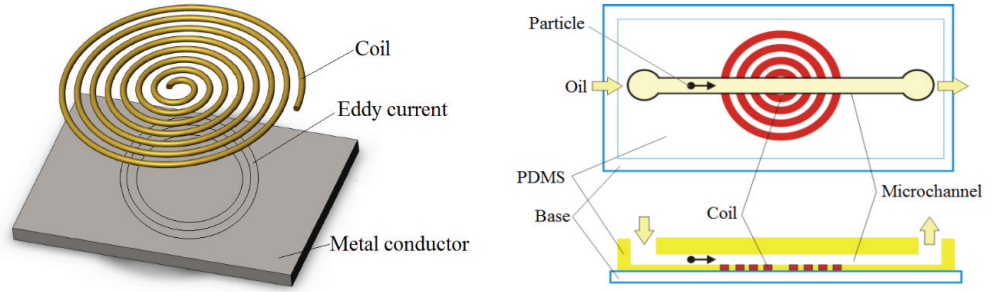

(a) (b)

Fig. 1. Schematic of the microfluidic chip for metal particle detection in oil

MODEL ESTABLISHMENT

Based on the detection principle described above, a mathematical model of the electromotive force ε induced in the metallic particle can be established as follows. B is the magnetic field intensity of the coil, and E_{in} is the electric field intensity induced in the particle. According to the Faraday law of electromagnetic induction, the induced electromotive force ε can be expressed as

$$\varepsilon = \oint_C \boldsymbol{E}_{in} \bullet d\boldsymbol{l} = -\frac{d\phi}{dt} = -\frac{d}{dt}\iint_S \boldsymbol{B} \bullet d\boldsymbol{S} = -\iint_S \left(\frac{\partial \boldsymbol{B}}{\partial t} \bullet d\boldsymbol{S} + \boldsymbol{B} \bullet \frac{\partial}{\partial t} d\boldsymbol{S} \right) \tag{2}$$

The first term on the right-hand side is the magnetic field with respect to time, εt, and the second term on the right-hand side is the closed-loop eddy current with respect to time, ε_m. Thus, the induced electromotive force ε can be divided into the following components:

$$\varepsilon_t = -\frac{d\phi_t}{dt} = -\iint_S \frac{\partial \boldsymbol{B}}{\partial t} \bullet d\boldsymbol{S} \tag{3}$$

$$\varepsilon_m = -\frac{d\phi_m}{dt} = -\iint_S \boldsymbol{B} \bullet \frac{\partial}{\partial t} d\boldsymbol{S} \tag{4}$$

The movement of the closed loop forming the eddy current is illustrated in Figure 2.

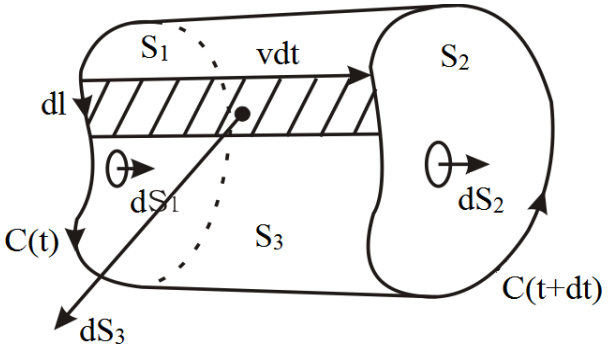

Fig. 2. Movement of the closed loop inside the particle

It is assumed that the closed loop C moves from C(t) to C(t+dt) at velocity *v* in dt. There are two different areas surrounded by C(t): S_1 and S_2+S_3. Thus, $d\Phi_m$ in Equation (4) can be expressed as

$$d\phi_m = \phi_{S_2} - \phi_{S_1} = \phi_{S_2} - (\phi_{S_2} + \phi_{S_3}) = -\phi_{S_3} \tag{5}$$

As seen from Figure 2, the effect of this movement on the magnetic flux can be expressed as

$$d\phi_m = -\phi_{S_3} = -\oint_C \boldsymbol{B} \bullet (dl \times \boldsymbol{v})\, dt \tag{6}$$

The effect of the movement on the induced electromotive force εm can then be expressed as

$$\varepsilon_m = -\frac{d\phi_m}{dt} = \oint_C \boldsymbol{B} \bullet (dl \times \boldsymbol{v}) = \oint_C (\boldsymbol{v} \times \boldsymbol{B}) \bullet dl \tag{7}$$

According to the Stokes formula and Equation (7), Equation (2) can be expressed as:

$$\nabla \times \boldsymbol{E}_{in} = -\frac{\partial \boldsymbol{B}}{\partial t} + \nabla \times (\boldsymbol{v} \times \boldsymbol{B}) \tag{8}$$

It is assumed that the particle is moving in the x direction and that the magnetic field of the coil is uniformly distributed. B_1 is the magnetic field intensity of the coil due to the movement of the particle, and E_1 is the induced electric field intensity due to the movement of the particle; thus, Equation (9) can be obtained as follows:

$$\boldsymbol{B}_1(x,t) = \boldsymbol{B}(x - \boldsymbol{v}t, t) \tag{9}$$

From this equation, Equation (10) can be obtained:

$$-\frac{\partial \boldsymbol{B}_1}{\partial t} = -\frac{\partial \boldsymbol{B}}{\partial t} + \boldsymbol{v}\frac{\partial \boldsymbol{B}}{\partial x} \tag{10}$$

In Equation (10), $\boldsymbol{v}(\partial \mathbf{B}/\partial \mathbf{x})$ can be expressed as $(\boldsymbol{v}\bullet\nabla)$ B.

The equation for the transformation of the operator ∇ can be expressed as

$$\nabla\times(\boldsymbol{B}\times\boldsymbol{v}) = (\boldsymbol{v}\bullet\nabla)\boldsymbol{B} + (\nabla\bullet\boldsymbol{v})\boldsymbol{B} - (\boldsymbol{B}\bullet\nabla)\boldsymbol{v} - (\nabla\bullet\boldsymbol{B})\boldsymbol{v} \tag{11}$$

$\nabla\bullet\boldsymbol{B} = 0$ can be obtained according to the Maxwell equations, and the velocity $\boldsymbol{v}$ is a constant vector; thus, Equation (11) can be expressed as

$$\nabla\times(\boldsymbol{B}\times\boldsymbol{v}) = (\boldsymbol{v}\bullet\nabla)\boldsymbol{B} \tag{12}$$

Using Equation (12), Equation (10) can be expressed as

$$-\frac{\partial \boldsymbol{B}_1}{\partial t} = -\frac{\partial \boldsymbol{B}}{\partial t} + \nabla\times(\boldsymbol{B}\times\boldsymbol{v}) \tag{13}$$

According to the differential form of the Maxwell equations,

$$\nabla\times\boldsymbol{E}_1 = -\frac{\partial \boldsymbol{B}_1}{\partial t} \tag{14}$$

$$\nabla\times\boldsymbol{E} = -\frac{\partial \boldsymbol{B}}{\partial t} \tag{15}$$

Thus, Equation (13) can be expressed as

$$\nabla\times\boldsymbol{E}_1 = \nabla\times\boldsymbol{E} + \nabla\times(\boldsymbol{B}\times\boldsymbol{v}) \tag{16}$$

The electric field intensity due to the movement of the particle can then be expressed as

$$\boldsymbol{E}_1 = \boldsymbol{E} + \boldsymbol{v}\times\boldsymbol{B} \tag{17}$$

Equation (17) indicates that the electromotive force $\varepsilon = \oint_C \boldsymbol{E}\bullet d\boldsymbol{l}$ induced in the particle will increase as the velocity of the particle increases.

In addition, the inductance variation of coil is supposed to be expressed as below:

$$\Delta Z_{coil} = Z - Z_0 = jw\sum_{i=1}^{N}\iint_S \Delta B dS \tag{18}$$

$$\Delta L_{coil} = \frac{imag(\Delta Z_{coil})}{w} \tag{19}$$

According to Lenz's law, the direction of the induced electromotive force ε is opposite to that of the magnetic field of the coil. As a result, the inductance of the coil decreases with an increasing particle velocity.

The distribution of the magnetic flux density is evaluated by Comsol software based on the mathematical model, as discussed above. For instance, the magnetic flux density in the velocity of particle 5.8×10^{-3} m/s is shown in Figure3, the value of the magnetic field far away from the iron particle surface is 0.018 T in average, and the value at the surface of the particle is 0.04 T, and the value is increasing up to 0.05 T inside the particle, while the magnetic field is decreasing down to 0.001 T in the core region because of the skin effect of the high frequency magnetic field. According to Equation (18) and Equation (19), the inductance variation of coil are calculated with different magnetic flux density *B* and velocity of particles, as shown in Table 1

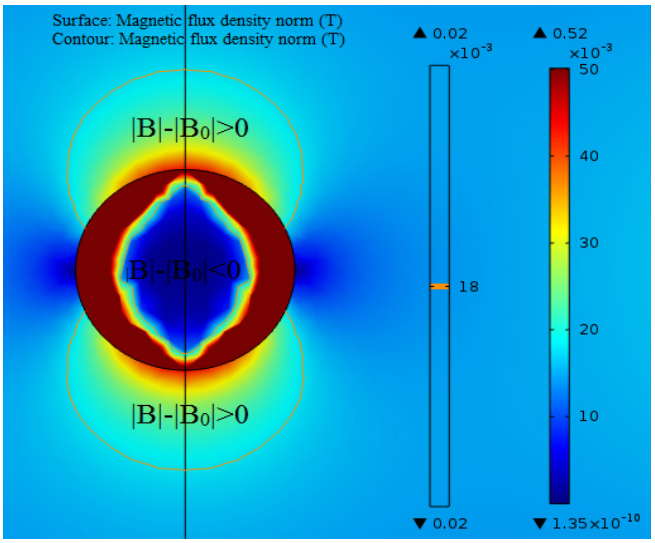

Fig.3. The distribution of magnetic flux density (vparticle= 5.8×10^{-3} m/s)

Table 1. The inductance variation of coil in different velocity of particles

Velocity of particles (m/s)	5.8×10^{-3}	1.16×10^{-2}	1.74×10^{-2}	2.32×10^{-2}	2.9×10^{-2}
Inductance variation of coil (nH)	0.85	0.75	0.66	0.53	0.46

EXPERIMENTAL VALIDATION

First, a mold for a chip with a microfluidic channel was fabricated using copper wire with a diameter of 270 μm, and a one-layer planar coil was fabricated with 33 turns of copper wire with a diameter of 50 μm. Second, casting material for the chip was fully mixed at a 10:1 ratio of liquid polydimethylsiloxane (PDMS) and curing agent. Then, the mold was filled with the liquid PDMS and placed in an incubator with a thermostat. The incubator was heated to 60^{O}C and maintained at

this temperature for two hours. Third, the solid PDMS was trimmed, and the mold of the fluidic channel was removed. Finally, a glass substrate was installed after the plasma cleaning of the bottom of the chip and the surface of the glass slide. A photograph of the final microfluidic chip is shown in Figure 4.

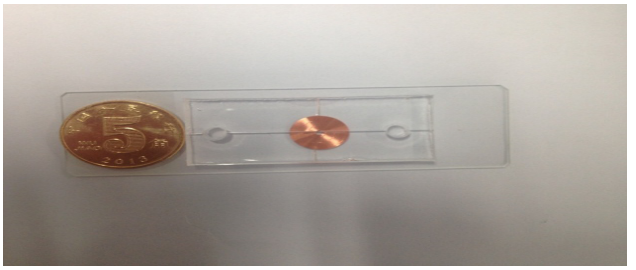

Fig. 4. Photograph of the microfluidic detection chip

As shown in Figure 5, the experimental system consisted of a syringe pump (Harvard Apparatus, 70-2212), the fabricated microfluidic chip, an inductance-capacitance-resistance (LCR) meter (Agilent E4980A, Santa Clara, CA) and a computer. LabVIEW® was used to stabilize the measured inductance signals. A 2 V, 2 MHz AC voltage was supplied by the LCR meter. For each test, a mass of 10 mg of particles was weighed using a precision balance (XS225A, precision: 0.1 mg) and then mixed with 50 mL of Hyspin AWS 10 hydraulic oil. Iron particles (Shahong Electromechanical Technology Company, Hefei, China) with a diameter of 80 μm are applied for the test.

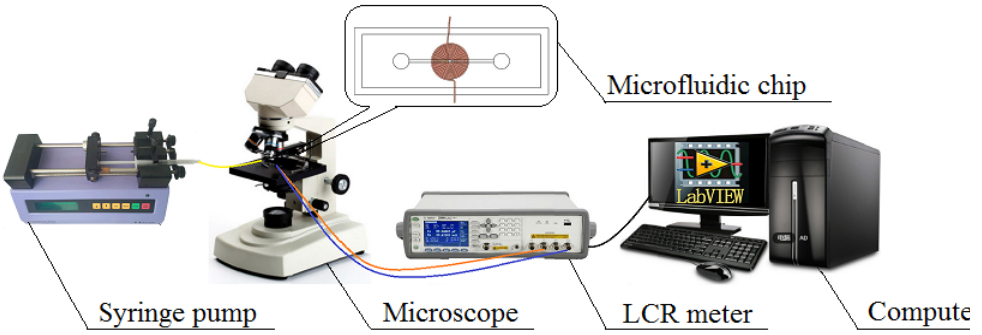

Fig. 5. Diagram of the detection system

The movement of the particles was controlled by the syringe pump, and the volume flows of the syringe pump were set to 0.02 mL/min, 0.04 mL/min, 0.06 mL/min, 0.08 mL/min and 0.10 mL/min, corresponding to particle velocities of 5.8×10^{-3} m/s, 1.16×10^{-2} m/s, 1.74×10^{-2} m/s, 2.32×10^{-2} m/s and 2.9×10^{-2} m/s, respectively.

In the experiments, 4 groups of tests were recorded at each velocity. The other parameters - i.e., temperature, particle size, voltage of the excited signal, frequency of the excited signal, etc. - were held constant.

The numerical experimental data and the trace of the inductive pulses in the coil at a particle velocity of 5.8×10-3 m/s are shown in Table 2 and Figure 6, respectively. According to Table 2, the

average inductance variation of the coil was 0.81 nH at a particle velocity of 5.8×10^{-3} m/s. Similar inductive pulses in the coil recorded at particle velocities of 1.16×10^{-2} m/s, 1.74×10^{-2} m/s, 2.32×10^{-2} m/s and 2.9×10^{-2} m/s are shown in Figure 7.

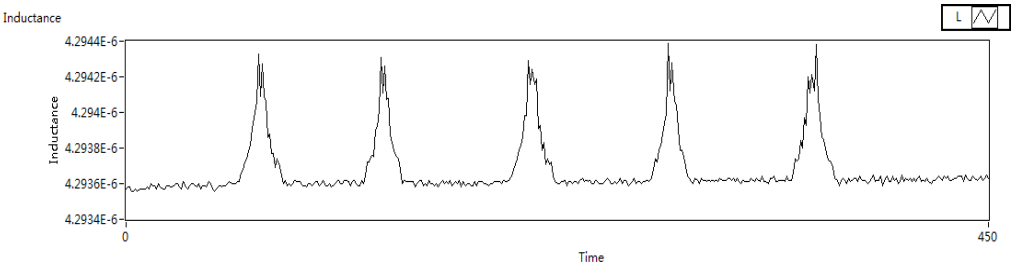

Fig. 6. Inductive pulses in the coil at a particle velocity of 5.8×10^{-3} m/s in test 1

Table 2. Experimental data recorded at a particle velocity of 5.8×10^{-3} m/s

Test number	1	2	3	4
Base inductance of coil (μH)	4.29357	4.29357	4.29357	4.29357
Maximum inductance of coil (μH)	4.29439	4.29436	4.29439	4.29438
Inductance variation of coil (nH)	0. 81786	0. 78786	0. 81786	0. 80786
Average inductance variation of coil (nH)		0. 807857		
Standard deviation of inductance variation (nH)		0.001414214		

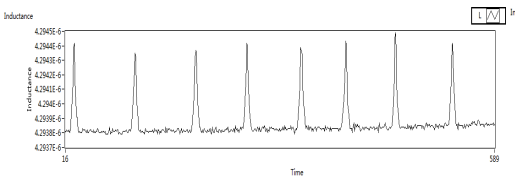

(a) 1.16×10^{-2}m/s

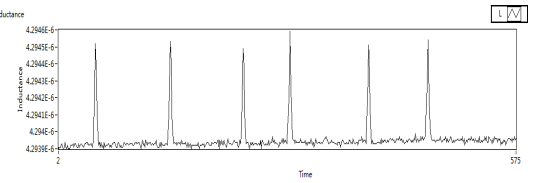

(b) 1.74×10^{-2}m/s

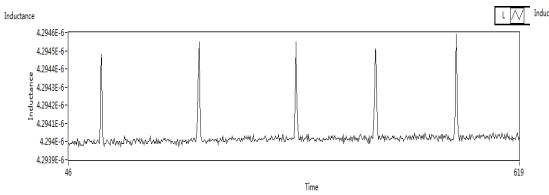

(c) 2.32×10^{-2}m/s

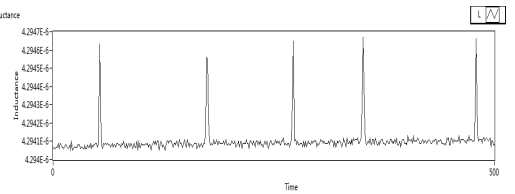

(d) 2.9×10^{-2}m/s

Fig. 7. Inductive pulses in the coil recorded at various particle velocities

The numerical experimental data recorded at all different particle velocities are summarized in Table 3. In this table, the rates of inductance variation of the coil for the different velocities are calculated with respect to the average inductance variation of the coil at a particle velocity of 2.9×10^{-2}m/s, which is treated as the reference.

Table 3. Summary of the experimental data

Volume flow (mL/min)	**0.02**	**0.04**	**0.06**	**0.08**	**0.10**
Velocity of particles (m/s)	5.8×10^{-3}	1.16×10^{-2}	1.74×10^{-2}	2.32×10^{-2}	2.9×10^{-2}
Inductance variation of coil (nH)	0.807857	0.700833	0.6098	0.507885	0.430789
Rate of inductance variation of coil	87.52945%	62.68581%	41.55406%	17.89625%	0%
Standard deviation of inductance variation (nH)	0.00141421	0.00129099	0.00129099	0.00478714	0.00404145

As shown in Table 3, when the velocity of the particles was decreased from 2.9×10^{-2} m/s to 5.8×10^{-3} m/s, the magnitude of the inductance variation of the coil increased from 0.43 nH to 0.81 nH, corresponding to a sensitivity enhancement of 87.5%, and the standard deviation of the inductance variation decreased from 0.00404145 nH to 0.00141421 nH.

According to Table 1 and Table 3, the inductance variations including the experimental and simulation data, which are affected by the velocity of particles, are shown in Figure 8. The relationship between the rate of the inductance variations of coil and the velocity of particles is shown in Figure 9.

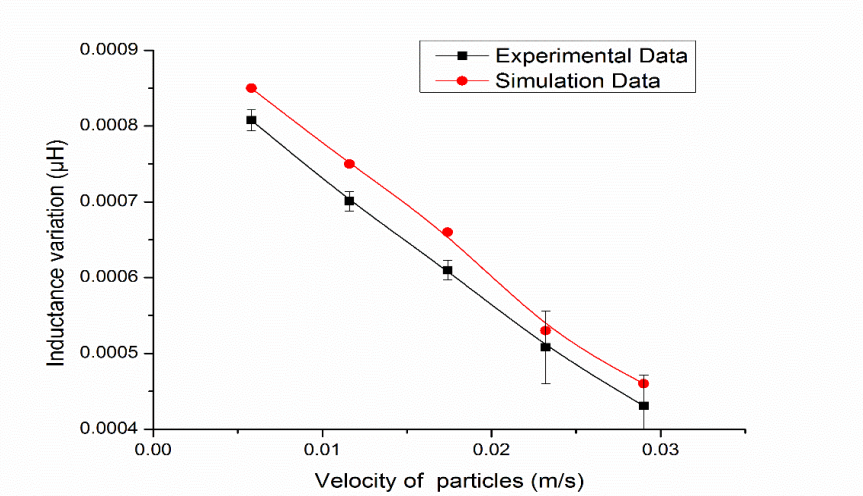

Fig. 8. Inductance variations affected by the velocity of particles

As shown in Figure 8, the differences of two data are between 4.6% and 8.9%, which is validated by comparing the experimental data with theory model. It is concluded that the inductance variation of coil increases and the standard deviation decreases as the velocity of particles decreases.

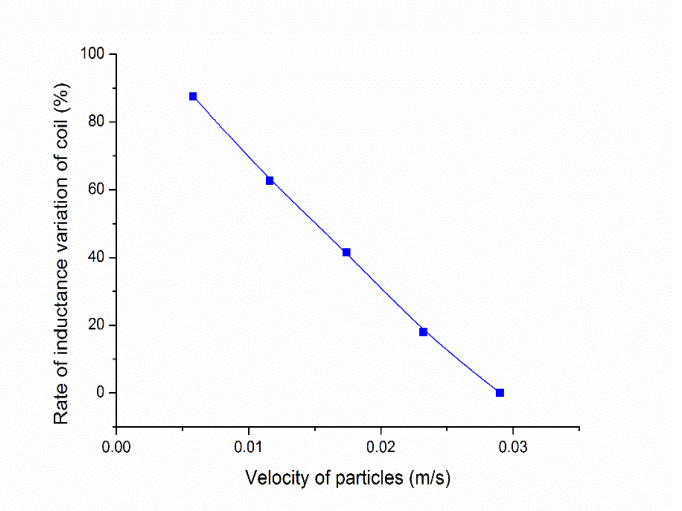

Fig. 9. Relationship between the rate of inductance variations of coil and the velocity of particles

According to the Figure 9, it is concluded that the rate of inductance variation decreases as the velocity of particles increases, and the relationship between them is an approximation of a linear dependency.

From the discussion above, it is recognized that the experiment resultis agreed with the theoretical analysis, and the sensitivity can be improved by decreasing the velocity of particle.

CONCLUSION

This paper presents research conducted to investigate the effect of the relative particle velocity on the signal pulses observed in inductive sensors. This work is expected to enable the improvement of inductive sensors in terms of their sensitivity for metal particle detection and in other aspects of their performance. A theoretical analysis and experiment validation are reported. Iron particle velocities of 5.8×10^{-3} m/s, 1.16×10^{-2} m/s, 1.74×10^{-2} m/s, 2.32×10^{-2} m/s and 2.9×10^{-2} m/s were investigated in the experiment. When the velocity of the particles was decreased from 2.9×10^{-2} m/s to 5.8×10^{-3} m/s, the inductance variation of coil increases from 0.43 nH to 0.81 nH, corresponding to a sensitivity enhancement of 87.5%, and the standard deviation of the inductance variation decreased from 0.00404 nHto 0.00141 nH. These results indicate that the sensitivity can be significantly improved by decreasing the velocity of particles, which is expecting to provide the guideline to improve the performance of the inductive sensor on metal particle detection and other application area.

REFERENCES

Aschenbrenner, B. & Agar, B.G. 2015. Analysis and validation of a planar high-frequency contactless absolute inductive position sensor. IEEE Transactions on Instrumentation and Measurement, 64(3):768-775.

Bakhoum, E.G. & Cheng, M.H.M. 2011. High-sensitivity inductive pressure sensor. IEEE Transactions on Instrumentation and Measurement, 60(8):2960-2966.

Bartsch, H., Geiling, T. & Muller, J. 2012. A LTCC low-loss inductive proximity sensor for harsh environments. Sensors and Actuators A-physical, 175:28-34.

Bera, S.C., Mandal, N. & Sarkar, R. 2011. Study of a pressure transmitter using an improved inductance bridge network and bourdon tube as transducer. IEEE Transactions on Instrumentation and Measurement, 60(4):1453-1460.

Cha, Y.J., Nam, B., Kim, J. & Kim, K.H. 2010. Evaluation of the planar inductive magnetic field sensors for metallic crack detections. Sensors and Actuators A-physical, 162(1):13-19.

Coskun, M.B., Thotahewa, K., Ying, Y.S., Yuce, M., Neild, A. & Alan, T. 2013. Nanoscale displacement sensing using microfabricated variable-inductance planar coils. Applied Physics Letters, 103(14):143501–143504.

Danisi, A., Masi, A., Losito, R. & Perriard, Y. 2013. Electromagnetic analysis and validation of an ironless inductive position sensor. IEEE Transactions on Instrumentation and Measurement, 62 (5):1267-1275.

Du, L., Zhe, J.A., Carletta, J., Veillette, R. & Choy, F. 2010. Real-time monitoring of wear debris in lubrication oil using a microfluidic inductive Coulter counting device. Microfluidics and Nanofluidics, 9(6):1241-1245.

Du, L., Zhu, X.L. & Zhe, J. 2014. A high sensitivity inductive sensor for blade tip clearance measurement. Smart Materials and structures, 23(6):065018-1–065018-9

Du, L., Zhu, X.L. & Zhe, J. 2015. An inductive sensor for real-time measurement of plantar normal and shear forces distribution. IEEE Transactions on Biomedical Engineering, 62(5):1316-1323.

Kejik, P., Kluser, C., Bischofberger, R. & Popovic, R.S. 2004. A low-cost inductive proximity sensor for industrial applications. Sensors and Actuators A-physical, 110(1):93-97.

Kim, K.C. 2013. Analysis on the characteristics of variable reluctance resolver considering uneven magnetic fields. IEEE Transactions on Magnetics, 49(7):3858-3861.

Kim, Y.H., Hashi, S., Ishiyama, K., Arai, K.I. & Inoue, M. 2000. Remote temperature sensing system using reverberated magnetic flux. IEEE Transactions on Magnetics, 36(5): 3643-3645.

Passeraub, P.A., Besse, P.A., de Raad, C., Dezuari, O., Quinet, F. & Popovic, R.S. 1998. Metallic profile and coin imaging using an inductive proximity sensor microsystem. Sensors and Actuators A-physical, 66(1):225-230.

Rahal, M. & Demosthenous, A. 2009. An ASIC front end for planar high-frequency contactless inductive position sensors. IEEE Transactions on Instrumentation and Measurement, 58(9):3021-3030.

Tang, Q.F., Peng, D.L., Wu, L. & Chen, X.H. 2015. An inductive angular displacement sensor based on planar coil and contrate rotor. IEEE Sensors Journal, 15(7):3947-3954.

Wei, H.Y. & Soleimani, M. 2012. Hardware and software design for a National Instrument-based magnetic induction tomography system for prospective biomedical applications. Physiological Measurement, 33(5):863-879.

Zhang, Z.J., Ni, F.L., Dong, Y.Y., Jin, M.H. & Liu, H. 2013. A novel absolute angular position sensor based on electromagnetism. Sensors and Actuators A-physical, 194:196-203.

Submitted: 29/Feb/2016
Revised : 15/Aug/2016
Accepted : 2/Nov/2016